Jarosław Janicki

University of Bielsko-Biała, Institute of Textile Engineering and Polymer Materials,
Willowa 2, 43-309 Bielsko-Biała, Poland.
e-mail: jjanicki@ath.bielsko.pl

Nanostructure of melt-processable molecular composites

Abstract

Novel melt-processable molecular composites were obtained from iPP and liquid crystalline oligoester (LCO). The nanostructure and thermal behaviour of these molecular composites were examined by a combination of real-time synchrotron SAXS/WAXD methods with differential scanning calorimetry (DSC). The synthesised oligoester with low melting temperature (118°C) exhibits the ability of forming a thermotropic mesophase. It was shown that stiff and strong rigid rod-like macromolecules of LCO are dispersed on the molecular scale in the iPP matrix and act as reinforcing fibres.

Key words: *melt-processable molecular composites: small-angle X-ray scattering; nanostructure; isotactic polypropylene, liquid crystalline oligoester*

1. Introduction

Small-angle X-ray scattering (SAXS) is a very useful technique for characterising inhomogeneous materials including polymers and nanocomposites on a nanometer scale.

Today, polypropylenes have become essential materials in fibre production for textiles and technical uses. However, both extremely high strength parameters and excellent dimensional stability are required for those fields of applications. In order to improve polymer properties, they are reinforced with glass fibres or with very high-strength and high-modulus liquid crystalline polymers. Liquid crystalline polymers are very stiff, which caused the enthalpy of mixing a rigid-rod polymer with a flexible chain to be mostly positive [1,2]. This generally leads to phase-separated systems. Recently, considerable efforts have been made by many researchers to obtain a new category of high-performance polymeric materials called molecular composites. Molecular composites consist of two polymeric components with dissimilar characteristics: a stiff and strong rigid-rod polymer dispersed at the molecular scale in a matrix of flexible polymer. During the last decade, liquid crystalline polymers (LCP) were presented as new compounds with superior properties, as compared to conventional polymers. The search for melt-processable liquid crystalline polymers which are miscible with conventional polymers is still a great challenge in polymer science [3]. Blending thermotropic LCP with semi-crystalline thermoplastic polymers to form *insitu* polymer composites is very attractive because of the advantages in lowering the viscosity during processing and in reinforcing the final mechanical properties [4]. However, the melting temperature of liquid crystalline polymers is usually too high for processing semi-crystalline thermoplastic polymers. In order to reduce the melting and transition temperature, new LCPs with flexible units in the main chain were synthesised, resulting in a decrease in melting temperature.

The aim of this paper is to present the results of the nanostructure investigations of molecular composites in non-isothermal conditions. The main interest is focused on the formation and changes of the supermolecular structure during the dynamic melting and crystallisation processes.

2. Experimental

2.1. Materials

Liquid crystalline compounds with three rings rod–like mesogen and aliphatic end groups were synthesised. The aromatic rings in the mesogen were bounded with ester groups, while the aliphatic end–groups consisting of eleven carbon atoms were connected with aromatic ring by ester bounds. The macromolecule chain of oligoester is presented in Figure 1.

The molecular composites were prepared from iPP and liquid crystalline oligoester (LCO) by mixing at the weight ratio of 80/20. The isotactic polypropylene used for investigations was commercial grade i-PP Chemopetrol (Czech Republic) with the density of 905 kg/m^3, melting temperature of 164°C and a melt flow index of MFI=2.5 g/min. The essential stages of molecular composites preparation were as follows: blending, extrusion and annealing at a constant temperature above the T_m of LCO and below the T_m of iPP.

2.2. Methods

The SAXS and WAXD investigations were carried out by means of a synchrotron beamline on the X33 double focusing camera of the EMBL in Hasylab, on the DORIS III storage ring of the DESY in Hamburg at a wavelength of 0.15 nm. The SAXS pinhole patterns of the LCO were recorded with a sample detector distance of 2.8 m to cover the range of modulus of the scattering vector of $0.012 \leq s \leq 0.894$ nm^{-1}, with s the modulus of the scattering vector ($s = 2\sin\theta/\lambda$, where 2θ is the scattering angle and λ is the wavelength). During the real-time measurements, the SAXS and WAXD patterns were simultaneously recorded every 6 seconds, corresponding to a resolution of one pattern per 1°C, using a standard acquisition system with two delay line detectors connected in series [5,6]. The range of scattering vectors was calibrated using the first nine orders of dry collagen with a spacing of 64 nm. The WAXD data was collected over the angular range of $11.7 \leq 2\theta \leq 46°$ calibrated with a silicon standard. The SAXS and WAXD intensities were normalised to the intensity of the primary beam and corrected for the detector response. Finally, an averaged melt pattern was subtracted from each curve to eliminate background scattering.

Differential scanning calorimetry measurements were carried out on a Perkin Elmer–Pyris unit, calibrated with the melting point of indium (156.6°C) and

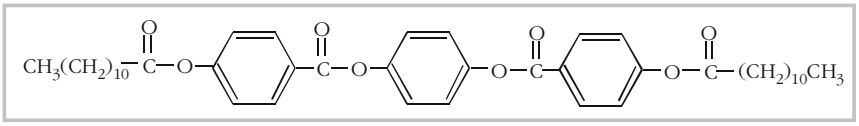

Figure 1. *The macromolecular chain of liquid crystalline oligoester.*

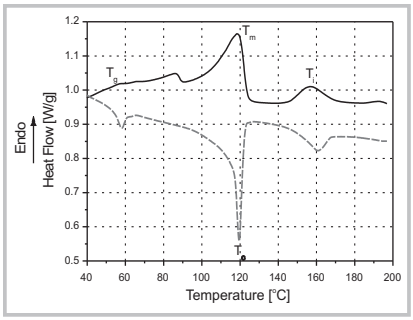

Figure 2. DSC heating and cooling curves for LCO, T_g, T_m, T_c, T_i are glass transition, melting, crystallisation and isotropisation temperature, respectively.

benzophenone (48°C) for the temperature, and with indium for the enthalpy (28.45 Jg^{-1}). The contribution of the empty pan was subtracted from each measurement. The block surrounding the measuring units was thermostatted at -10°C with liquid nitrogen, and the units was flushed with nitrogen. The heating and cooling rate of samples was 10°C / min.

3. Results and discussion

Information concerning the thermal behaviour of the liquid crystal oligoester was obtained by differential scanning calorimetry. DSC heating and cooling curves of oligoester at the rate of 10°C / min are shown in Fig. 2. The heating curves consist of three endotherm peaks. The first peak is connected with the glass transition temperature, which was evaluated as 40°C. The main endotherm peak indicates the melting temperature (118.7°C), and the third, the isotropisation temperature (156.6°C). When a cooling run is performed after initial heating, three exothermal peaks are observed.

Table 1. Transition temperature and anthalpy during heating and cooling.

Heating					Cooling			
T_g [°C]	$T_{m.}$ [°C]	ΔH_m [J/g]	T_i [°C]	ΔH_i [J/g]	T_c [°C]	ΔH_c [J/g]	T_i [°C]	ΔH_i [J/g]
40.6	118.7	17.5	156.6	2.3	114.8	-11.0	155	-2.6

where:
T_g, T_m, T_c, T_i are glass transition, melting, crystallisation and isotropisation temperatures respectively,
ΔH_m, ΔH_c, ΔH_i are the enthalpies of melting, crystallisation and isotropisation respectively,

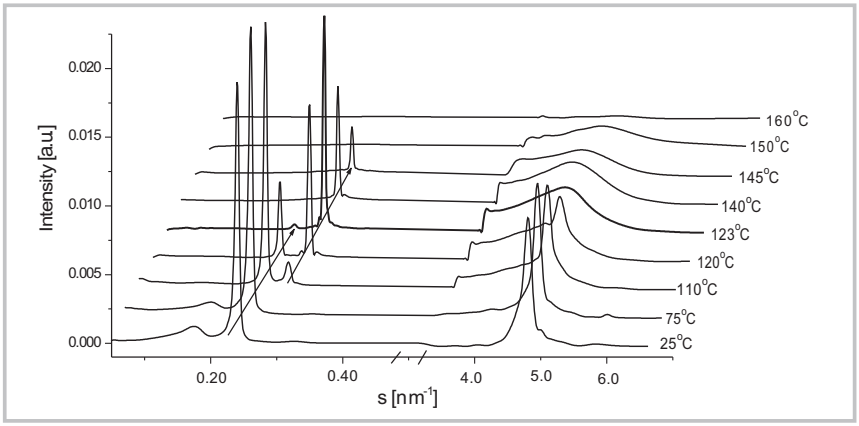

Figure 3. SAXS/WAXS patterns of LCO as a function of temperature during heating.

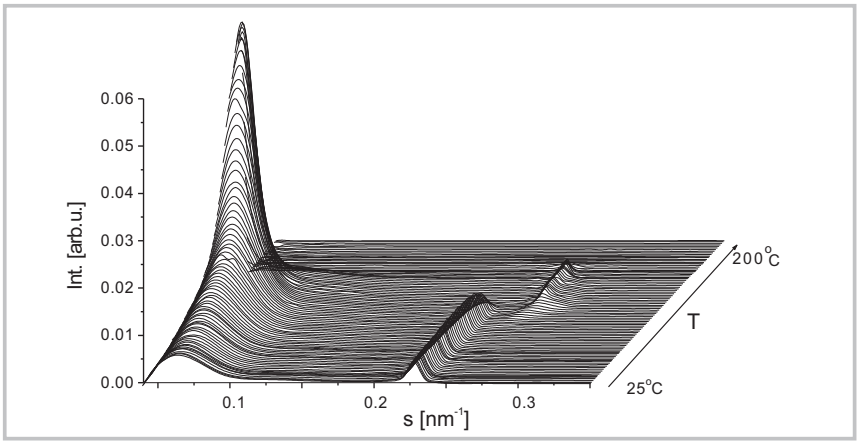

Figure 5. Small-angle diffraction patterns after background subtraction for LCO-iPP during heating at 10°C/min.

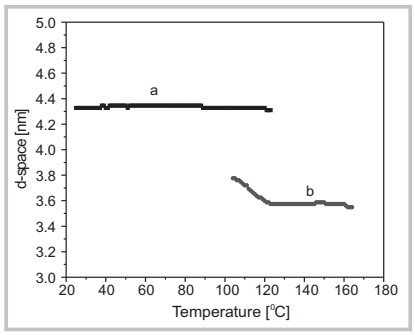

Figure 4. d–spacing for LCO.

The transition temperature and corresponding enthalpy during heating and cooling are presented in Table 1.

In order to determine the nanostructure of the oligoester, the WAXS and SAXS real-time synchrotron experiments were performed during heating and cooling at the rate of 10°C / min. The SAXS / WAXS patterns of liquid crystalline oligoester as a function of temperature during heating are presented in Fig. 3.

Based on a qualitative analysis, one can say that strong crystalline peaks on the WAXS curves observed from 25 to 123°C as well as the very low amorphous halo indicate a well-ordered structure. The crystalline peak disappears at 123°C, and the scattering curve at higher temperature indicates the liquid crystalline state. More structural parameters can be obtained from the SAXS investigations. The SAXS curves exhibit two distinct diffraction maxima, corresponding to a solid and liquid crystalline state respectively. The angular position of the peaks is connected with the supermolecular structure with different electron densities of phases, which are separated by a repeated distance. The values of the repeated distance (d-space) were evaluated using Bragg's law and are presented in Fig. 4. The values of the d-space calculated based on the angular position of the first SAXS peak are constant, and equal 4.33 nm (curve *a* in Fig. 4); they are characteristic for the solid state. Based on computer modelling, the length of the macromolecular chain was estimated as 4.2 nm, which is in good agreement with the result derived from the SAXS measurements. During the melting process, the macromolecular chains become more flexible

and the values of the d-space steadily decrease, as is shown in figure 4b. The equilibrium state appears at 123°C as the d-space is constant and equal to 3.57nm. The structure of the LCO examined under a polarising optical microscope (not reported in this paper) was identified as a smectic phase [7,8]. The two very sharp peaks on the SAXS curves and the corresponding changes of d-space are characteristic for the smectic liquid crystal structure, and confirm the result obtained from optical microscope observations.

To reveal the nanostructure of LCO-iPP molecular composite, time- and temperature dependent SAXS experiments were carried out. Small-angle scattering patterns of LCO-iPP after background subtraction during heating at 10°C / min are shown in Fig.5. One can see that the SAXS curves exhibit distinct diffraction maxima both from iPP lamellar structure and from LCO. The first peak at the initial temperature is located at s=0.07 nm^{-1}, corresponding to the long period of iPP. The second and third peaks occur at different temperature ranges, and correspond to the solid crystalline phase and liquid crystalline phase of the LCO respectively. During heating, the peak of iPP shifts to lower s-values, corresponding to larger values of the long period. At the same time, the intensities of the scattering maximum increases and the ratio of maximum intensity at 155°C to the intensity at 25°C are 12.5.

To monitor the evolution of the lamellar nanostructure of iPP during heating in the presence of LCO, the correlation functions [9,10] were calculated from real-time SAXS scattering curves. Based on the correlation functions, the values of long periods and crystalline lamellae thickness were determined. Changes in the long period during heating and corresponding changes of the thickness of crystalline lamellae are shown in Fig.s 6a and 6b respectively. It is seen that the values of the long period remain almost constant at about 13-14 nm below 100°C. A significant increase in long period value occurs above 100°C up to 30 nm at 160°C. It should be noted that the thickness of crystalline lamellae does not change considerably within the temperature range from 25 to 120°C; it remains almost constant at the level of 5.4 nm, then increases rapidly, reaching 9.5 nm at 160°C. One can suppose that such significant changes are caused by the influence of LCO on the recrystallisation process of iPP during isothermal annealing. The increase of the long period during heating can be explained by the fact that the thinner lamellae are melted first at lower temperature. The long period continues to increase drastically with temperature, until the thickest lamellae are melted. It was shown that changes in long periods during heating describe the exponential function, and the plot $\ln(L_p-L_{po})$ versus temperature gives the linear function (Fig.7) where L_{po} and L_p denote the value of the long period at the initial and given temperatures respectively. The slope of this function is connected with the kinetic of the melting process of the lamellar structure. The slope for pure iPP is higher than for LCO-iPP, which indicates that the LCO prevents the iPP lamellae from melting. As a consequence, the thickest lamellae are melted at the temperature range 120-160°C in the presence of the liquid crystalline phase of LCO.

4. Conclusions

In summary, this study indicates that synthesised oligoester exhibits the ability of thermotropic mesophase formation. The solid crystalline state of LCO is observed in the temperature range of 25 to 123°C, and the liquid crystalline state in the temperature range 118-156°C. Real-time synchrotron SAXS and WAXD measurements allowed the phase transition of LCO to be determined, and indicated the smectic type of mesophase. Due to low melting temperature and the wide temperature range of mesophase, oligoester can be used as a proper compound for processing with iPP. Changes in the nanostructure parameters of iPP during heating and cooling give evidence that the nanostructure is influenced by the presence of LCO. The stiff and strong rigid rod-like macromolecules of LCO are dispersed at the molecular scale in the iPP matrix and act as reinforcing fibres [11].

Based on the results obtained, we can assume that liquid crystalline oligoester is dispersed homogenously in the iPP matrix giving the molecular composites. The results suggest that the proposed approach may be practicable in preparing a melt-processable molecular composite.

❑

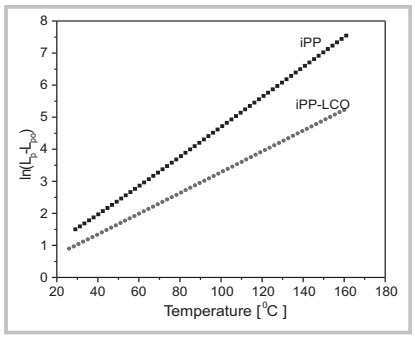

Figure 7. The plot of $\ln(L_p-L_{po})$ versus temperature.

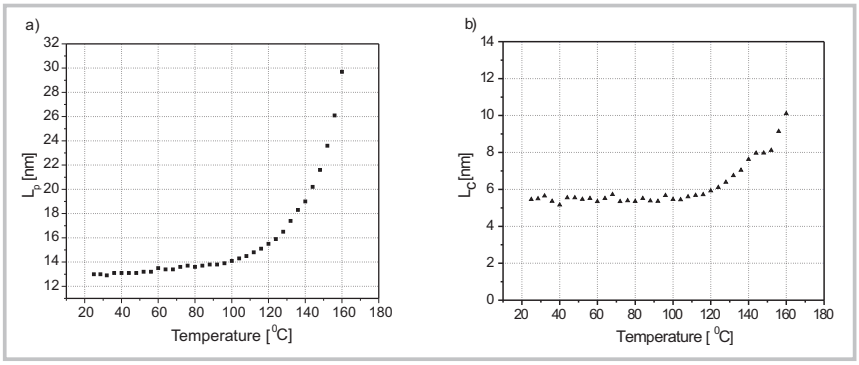

Figure 6. The supermolecular structure parameters determined from correlation functions for iPP during heating of LCO-iPP: a) long period L_p, b) thickness of crystalline lamellae L_c

Acknowledgment

The author thanks Professor Harry Reynaers, Dr Bart Goderis and Dr. M. Koch for help during synchrotron measurements and for their fruitful discussions.

References

1. *Ho, J. & Wei, K. (2000). Macromolecules, 33, 5181-5186*
2. *Ho, J. & Wei, K. (2201). J. Polym. Sci., Polym. Phys. Ed. 38, 2124*
3. *Takayanagi, M., Ogata, T., Morkawa, M., & Kai, T. (1980). J. Macromol. Sci.-Phys. B17(4), 591*
4. *Costa, G., Meli, D., Song, Y., Turturro, A., Valenti, B., Castellano, M. & Falqui, L. (2001). Polymer 42, 8035*
5. *Koch, M.H.J. & Bordas, J. (1985). Nucl. Instrum. and Methods, 208, 461*
6. *Boulin, C.J., Kempf, R.,Gabriel, A.,& Koch, M.H.J. (1995). Nucl. Instrum. and Methods, A357, 178*
7. *Grebowicz, J. & Wunderlich, B. (1983). J. Polym. Sci., Polym. Phys. Ed. 21, 141*
8. *Janicki, J. (2002). Acta Physica Polonica 101(5), 761-766*
9. *Vonk, C. G. Kortleve, G. (1967). Kolloid – Z.Z. Polymer, 220, 19*
10. *Goderis, B., Reynaers H., Koch, M. H. J. & Mathot, V. B. F. (1999) J. Polym. Sci. Polym. Phys. 37, 1715*
11. *Schartel, B. & Wendorff, J. H. (1999). Polymer Engineering and Science 39(1), 128-151*

❑ ***Received 14.01.2003, Revieved 05.05.2003***